Eur. Phys. J. A **17**, 423–428 (2003)
DOI 10.1140/epja/i2002-10186-5

THE EUROPEAN PHYSICAL JOURNAL A

Proton knock-out in Hall A

K. de Jager[a]

For the Jefferson Lab Hall A Collaboration
Jefferson Lab, Newport News, VA 23606, USA

Received: 1 November 2002 /
Published online: 15 July 2003 –

Abstract. Proton knock-out is studied in a broad program in Hall A at Jefferson Lab. The first experiment performed in Hall A studied the ^{16}O$(e,e'p)$ reaction. Since then proton knock-out experiments have studied a variety of aspects of that reaction, from single-nucleon properties to its mechanism, such as final-state interactions and two-body currents, in nuclei from ^{2}H to ^{16}O. In this review the accomplishments of this program will be summarized and an outlook given of expected future results.

PACS. 25.30.Rw Electroproduction reactions – 24.70.+s Polarization phenomena in reactions

1 Introduction

Coincident electron-induced proton knock-out experiments have long served as precision tools for the study of the nuclear electromagnetic response. Cross-section data have been used to test the mean-field model of protons bound inside the nucleus and to study their wave function. For example, the extensive program at NIKHEF has established that the spectroscopic factor, the integrated single-particle strength, is quenched by 30–40% throughout the periodic table. The missing strength is assumed to have been shifted to high values of missing energy $E_{\rm m}$ and momentum $p_{\rm m}$ through nucleon-nucleon correlations. Separated response functions have provided detailed information on the various components of the reaction mechanism, such as Final State Interactions (FSI), Meson-Exchange Currents (MEC), Isobar Currents (IC) and the effects of relativity.

Hall A at Jefferson Lab is equipped with a pair of identical high-resolution spectrometers, which combine a high momentum resolution ($1.5 \cdot 10^{-4}$) to a sizeable angular (6 msr) and momentum ($\pm 5\%$) acceptance. Detailed information on the Hall A instrumentation is available in ref. [1]. In conjunction with the beam properties out of the CEBAF accelerator [2] ($E_{\rm max} \approx 6$ GeV, $I_{\rm max} \approx 100$ μA and polarization $\geq 70\%$), this provides the perfect environment for a broad and in-depth program of $(e,e'p)$ studies. The high beam energy and luminosity make it possible to cover large Q^2, $p_{\rm m}$ and $E_{\rm m}$ ranges at a variety of kinematics (parallel and perpendicular). Various nuclei from ^{2}H to ^{16}O have been investigated.

[a] e-mail: kees@jlab.org

2 Formalism

The kinematics for the $(e,e'p)$ reaction are shown in fig. 1. The scattering plane is defined by the incoming electron, $k^\mu = (E_e, \mathbf{k})$, and the outgoing electron, $k'^\mu = (E'_e, \mathbf{k}')$. The four-momentum of the virtual photon is given by $q^\mu = (\omega, \mathbf{q})$ and the four-momentum of the outgoing proton is given by $p'^\mu = (E_p, \mathbf{p}')$. The four-momentum square, $Q^2 = q^2 - \omega^2$, is defined such that Q^2 is always positive for electron scattering. The missing-momentum vector is defined as $\mathbf{p}_{\rm m} = \mathbf{q} - \mathbf{p}'$ and represents the momentum of the recoiling system. In polarization transfer reactions $(\vec{e},e'\vec{p})$ the components of the polarization of the knocked-out proton are defined relative to $\mathbf{q}$ in the coordinate system indicated in the figure.

The form of the differential cross-section for $(e,e'p)$ reactions in the one-photon exchange approximation without polarization is

$$\frac{{\rm d}^6\sigma}{{\rm d}\Omega_{e'}{\rm d}E_{e'}{\rm d}\Omega_{p'}{\rm d}E_{p'}} = \frac{E_p p'}{(2\pi)^3}\sigma_{\rm Mott}[v_T R_T + v_L R_L + v_{LT} R_{LT}\cos\phi_{pq} + v_{TT} R_{TT}\cos 2\phi_{pq}]\,, \quad (1)$$

with ϕ_{pq} the angle between the plane defined by $\mathbf{e}$ and $\mathbf{e}'$ and the plane defined by $\mathbf{p}'$ and $\mathbf{q}$, and $\sigma_{\rm Mott}$ the Mott cross-section,

$$\sigma_{\rm Mott} = \frac{4\alpha^2 E_{e'}^2}{Q^4}\cos^2\frac{\theta_e}{2}. \quad (2)$$

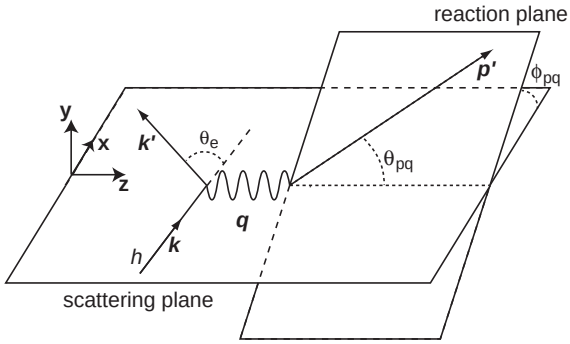

Fig. 1. A schematic of the kinematics for the $(e, e'p)$ reaction.

The kinematics factors v_L, v_T, v_{LT},and v_{TT} are:

$$v_L = \frac{Q^4}{q^4}\,, \tag{3}$$

$$v_T = \frac{Q^2}{2q^2} + \tan^2(\theta_e/2)\,, \tag{4}$$

$$v_{LT} = \frac{Q^2}{q^2}\left[\frac{Q^2}{q^2} + \tan^2(\theta_e/2)\right]^{1/2}, \qquad \text{and} \tag{5}$$

$$v_{TT} = \frac{Q^2}{2q^2}\,. \tag{6}$$

The response functions, R_L, R_T, R_{LT}, R_{TT}, can be separated by a suitable choice of the kinematic parameters. In perpendicular in-plane kinematics with a fixed $\mathbf{q}$ and ω, one can separate R_T, R_{LT}, and a combination of the R_L and R_{TT} response functions, denoted as R_{L+TT}. One can also measure the cross-section asymmetry A_{LT} for a given $\mathbf{q}$ and ω. This asymmetry is defined as

$$A_{LT} = \frac{\sigma(\phi = 180^\circ) - \sigma(\phi = 0^\circ)}{\sigma(\phi = 180^\circ) + \sigma(\phi = 0^\circ)}\,. \tag{7}$$

In parallel and anti-parallel kinematics, *i.e.* when the outgoing proton is in the direction of $\mathbf{q}$, one can separate the R_L and R_T response functions. In parallel kinematics $\mathbf{p}_\mathrm{m}$ points in the opposite direction as $\mathbf{q}$ with $x_\mathrm{B} < 1$, while in anti-parallel kinematics $\mathbf{p}_\mathrm{m}$ points in the same direction as $\mathbf{q}$ with $x_\mathrm{B} > 1$, where

$$x_\mathrm{B} = \frac{Q^2}{2M\omega} \tag{8}$$

is the Bjorken scaling variable. For $x_\mathrm{B} > 1$, the region in ω between the quasi-elastic peak and the elastic peak is being probed; while for $x_\mathrm{B} < 1$, the region in ω towards the Δ-resonance is being probed. The region in ω between the quasi-elastic peak and Δ-resonance is often referred to as the dip region.

3 Many-body systems

The $(e, e'p)$ reaction has been used for many decades to test a mean-field description of a nucleus. The first experiment carried out in Hall A at Jefferson Lab was E89-003 [3], a study of $^{16}\mathrm{O}(e, e'p)$ at a constant value of the four-momentum transfer squared Q^2 of 0.8 $(\mathrm{GeV}/c)^2$ and $\omega = 439$ MeV. For $p_\mathrm{m} \leq 350$ MeV/c, the response functions R_{L+TT}, R_T and R_{LT} were separated and A_{LT} was extracted for 1p-shell knock-out.

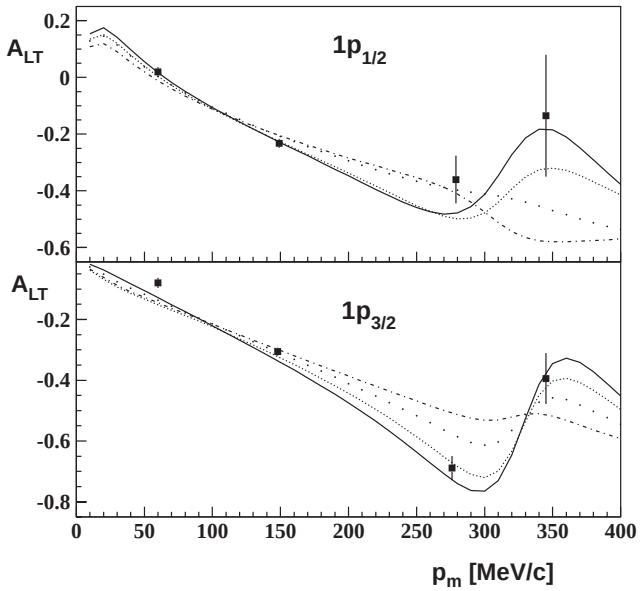

Fig. 2. Measured left-right asymmetry A_{LT} and DWIA calculations for knock-out from the 1p-shell. All curves are from Udias [5]. The solid line is the fully relativistic calculation. The densely dotted line is the calculation with only the bound-state spinor distortion included, the loosely dotted line that with only the scattered-state spinor distortion included. The dot-dashed line is the calculation without any spinor distortion. The error bars shown are the quadratic sum of the statistical and systematic uncertainties.

The ~ 70 μA continuous electron beam with an energy of 2.4 GeV was scattered from a waterfall target with three foils, each ~ 130 mg/cm^2 thick. The scattered electrons and the knocked-out protons were detected in coincidence in the two high-resolution spectrometers. A missing-energy resolution of 0.9 MeV FWHM was obtained. The angle of any tracked particle was determined to 0.3 mrad, and its momentum with a relative accuracy of $1.5 \cdot 10^{-3}$. The absolute efficiency for the coincident cross-section data was determined by comparing the elastic hydrogen cross-section, obtained simultaneously from the waterfall target, to the available world data.

The results for knock-out from the 1p-shell [4] have been compared to full Relativistic Distorted Wave Impulse Approximation (RDWIA) calculations by Udias [5]. In the full RDWIA approach the Dirac equation was solved directly in configuration space. The Coulomb gauge, the cc2 current operator, the NLSH mean-field bound-state wave function [6] and the energy-dependent optical model parametrization of Cooper *et al.* [7] were used. Similar calculations by Kelly [8] produced identical results. The results for the asymmetry A_{LT} are shown in fig. 2. There is a large change in the slope of A_{LT} evident at $p_\mathrm{m} \approx 300$ MeV/c. In Udias' calculations the nucleon current is computed with a fully relativistic operator. The

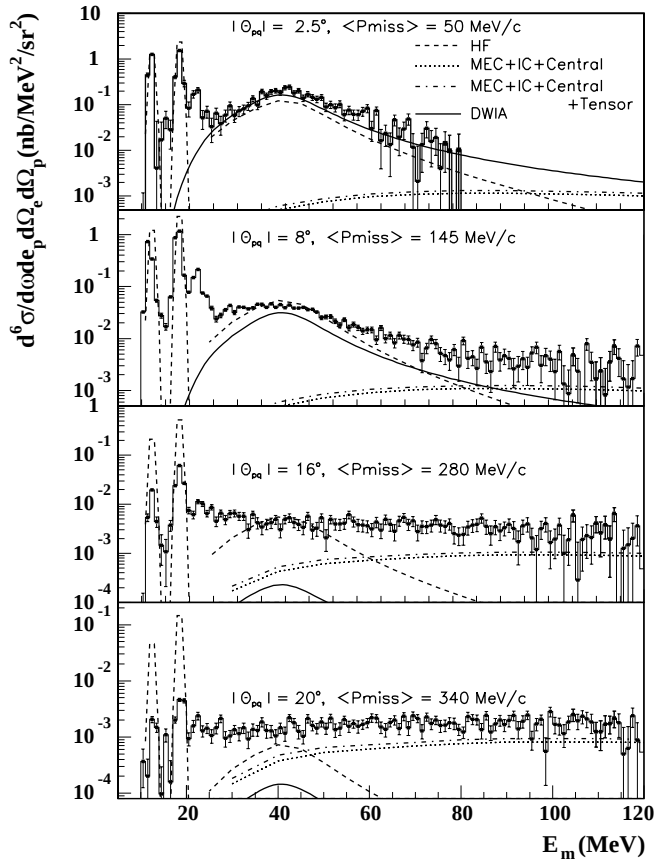

Fig. 3. The cross-section measured at different outgoing-proton angles as a function of missing energy, averaged over the values measured at either side of **q**. The curves show the single-particle strength calculated by Kelly [10] (solid curve, only the *s*-shell is shown) and by Ryckebusch (dashed curve), folded with the Lorentzian parametrization of Mahaux. The dotted line shows the Ryckebusch calculation of the $(e, e'pn)$ and $(e, e'pp)$ contributions to the $(e, e'p)$ channel including MEC and IC contributions and central correlations, while the dot-dashed line also includes tensor correlations.

effect of spinor distortions on A_{LT} is evident from the curves in which the enhancement of the lower components is artificially removed. Clearly, a fully relativistic calculation is required to reproduce the slope change in A_{LT} observed at high $p_{\rm m}$ values.

Figure 3 shows the cross-section [9] measured up to $E_{\rm m}$ values of 120 MeV as a function of $p_{\rm m}$. At the lowest $p_{\rm m}$ value (50 MeV/c) a wide peak is evident at $E_{\rm m} \approx 40$ MeV, due predominantly to knock-out of $1s_{1/2}$ protons. This peak decreases with increasing $p_{\rm m}$ and has disappeared beneath a flat background for $p_{\rm m} \geq 200$ MeV/c. The continuum knock-out results have been compared to single-particle knock-out calculations by Kelly [10]. These DWIA calculations used a relativized Schrödinger equation and spread the cross-section (normalized by a factor of 0.73) over $E_{\rm m}$ using a Lorentzian parametrization. At small $p_{\rm m}$ this model describes the data well, but at larger $p_{\rm m}$ the DWIA cross-section is much smaller than the data. Figure 3 also shows the results of $(e, e'pn)$ and $(e, e'pp)$ calculations by Ryckebusch [11] in a Hartree-Fock framework. In his calculations FSI effects were neglected, but MEC, IC and tensor correlations were included. The flat cross-section observed is confirmed by Ryckebusch, but at approximately half the observed strength, with the main contribution coming from two-body currents. Ryckebusch' calculations shown in the figure strongly overestimate knock-out from the valence orbits at higher $p_{\rm m}$. In more recent calculations he has replaced the rescattering optical potential by the Glauber multiple-scattering theory, an approach better suited to the higher proton momenta in the JLab experiments. Preliminary results yield agreement with the data over the complete experimental $E_{\rm m}$ and $p_{\rm m}$ ranges.

A follow-up experiment, E00-102 [12], was completed a year ago. Cross-section measurements and response function separations were performed at the same Q^2 value as E89-003 (0.8 (GeV/c)^2). For small $E_{\rm m}$ values a $p_{\rm m}$ range from -500 MeV/c to $+750$ MeV/c was studied, while for $E_{\rm m}$ up to 170 MeV data were taken at $p_{\rm m}$ values between 70 and 350 MeV/c.

4 Few-body systems

The ^{2}H$(e, e'p)n$ reaction is ideal to investigate the short-range structure of the (NN) interaction, which determines the high-momentum components of the deuteron wave function. The first experiment to study those aspects was E94-004 [13], which measured the cross-section on roughly the quasi-elastic peak at $Q^2 = 0.665$ (GeV/c)^2. The missing energy $p_{\rm m}$ was varied from 0 to 500 MeV/c by changing the proton angle. Since the electron kinematics were kept fixed, the electron spectrometer was used to monitor the product of target density and detector dead time. The total systematic uncertainty in the absolute cross-section was estimated to be less than 10%.

The data [14] were compared to calculations by Ritz *et al.* [15], which included relativistic contributions of leading order in $p_{\rm m}$ to the kinematic boost of the wave function and to the nucleon current. The Bonn (NN) potential and dipole nucleon form factors were used. The full calculation is in good agreement with the data for $p_{\rm m} \geq 400$ MeV/c, where FSI and IC effects contribute up to 100%. However, at smaller $p_{\rm m}$ values the calculations undershoot the data by up to 20%.

To investigate the origin of this discrepancy, experiment E01-020 [16] was carried out this year. In this experiment the ^{2}H$(e, e'p)$ cross-section was measured and the R_{LT} response function separated for $p_{\rm m}$ up to 500 MeV/c at three Q^2 values of 0.8, 2.1 and 3.5 (GeV/c)^2. At constant $p_{\rm m}$ values of 200, 400 and 500 MeV/c the cross-section has been measured as a function of the angle of the recoiling neutron with respect to **q** between 20° and 150°. This corresponds to a range in $x_{\rm B}$ between 0.7 and 1.5, which allows a detailed study of FSI effects. Measurements at a small $p_{\rm m}$ value of 50 MeV/c will serve as normalization, since FSI, MEC and IC effects are expected to be small there.

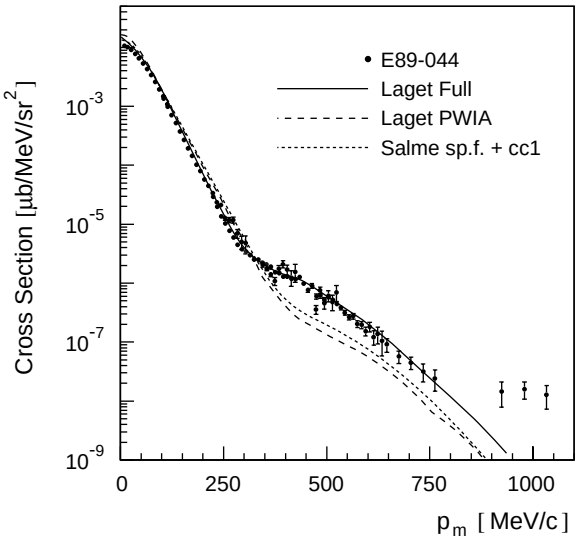

Fig. 4. Preliminary results for the ^{3}He$(e,e'p)d$ cross-section as a function of p_m. The curves show the latest calculation by Laget [18] together with a PWIA one by Salme [20].

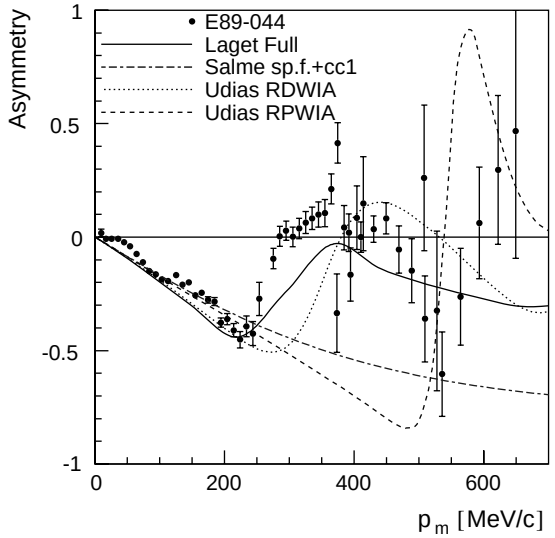

Fig. 5. Preliminary A_{LT} data for ^{3}He as a function of p_m. The curves show the latest calculation by Laget [18] along with preliminary results from Udias [5] and a PWIA calculation by Salme [20].

In the E89-044 experiment [17] on ^{3}He different kinematic regions were studied, each focusing on a particular aspect of the nuclear structure or of the reaction mechanism. In constant ($q = 1.5$ GeV/c, $\omega = 0.845$ GeV) kinematics the single-nucleon structure of ^{3}He was studied up to $p_\mathrm{m} = 1$ GeV/c. The response functions R_{L+TT}, R_T and R_{LT} were separated up to $p_\mathrm{m} = 550$ MeV/c. To investigate the Q-dependence of the reaction mechanism, the R_L and R_T structure functions were separated in parallel kinematics up to 3 GeV/c, for $p_\mathrm{m} = 0$ MeV/c and for $p_\mathrm{m} = \pm 300$ MeV/c at $Q = 1$ and 2 GeV/c. In the continuum region a full in-plane separation of R_L and R_T was performed to search for correlated nucleon pairs.

Preliminary results for the cross-section in the two-body reaction channel are shown in fig. 4 in forward perpendicular kinematics. The most recent calculations by Laget [18] yield an excellent description of the data up to $p_\mathrm{m} = 750$ MeV/c. Laget's calculations are based on the diagrammatic method which he has developed for the analysis of photo- and electro-production of the three-nucleon system [19]. The kinematics and the phase space are relativistic, while the energy and momentum are conserved at each vertex. For the ^{3}He and ^{2}H wave functions solutions of the Faddeev equations for the Hannover 18 three-body and the Paris two-body potentials, respectively, are used. A complete set of two-body matrix elements includes both possible isospin states and the charge-exchange mechanism. The meson scattering amplitude relates the ^{3}He three-body break-up and the subsequent ^{2}H recombination matrix elements. The half off-shell nucleon-nucleon rescattering amplitude was originally expanded in terms of partial waves up to and including D-waves. Recently, Laget has introduced the Glauber multiple-scattering theory, in which the FSI are calculated directly from the elementary nucleon-nucleon scattering amplitudes, better suited for the higher proton momenta of the present experiments. The total nucleon-nucleon scattering cross-section has a minimum at a proton kinetic energy $T_p \approx 200$ MeV, then rises and reaches a plateau for $T_p \geq 800$ MeV. For $50 \leq p_\mathrm{m} \leq 200$ MeV/c, there is good agreement between the data and both PWIA calculations [18,20] and the DWIA calculation [18]. At $p_\mathrm{m} \leq 50$ MeV/c the data exceed the calculations by similar amounts as for ^{2}H. At the highest p_m values the measured cross-section is up to an order of magnitude larger than the calculated one.

The preliminary results for A_{LT} are shown in fig. 5. The curves represent the same calculations by Laget, shown in the previous figure, as well as the preliminary results of Udias [5]. Both the RDWIA and the RPWIA calculations used a mean-field approximation. Udias is working on the inclusion of realistic three-body wave functions in his code. At intermediate p_m values, A_{LT} is sensitive to relativistic effects, while at the highest p_m values FSI effects dominate.

A variety of realistic models [21,22] predict a sharp minimum in the spectral function of ^{4}He at a missing-momentum value $p_\mathrm{m} \approx 400$ MeV/c, which is directly attributed to short-range calculations. Similar calculations for ^{3}He do not show a sharp minimum, but that is due to the d-state component in the ^{3}He wave function. In practice the minimum for ^{4}He can easily be filled by reaction mechanism effects [18,22] at lower Q^2 values. An earlier experiment at NIKHEF [23] indeed failed to observe such a minimum at a constant ($q = 400$ MeV/c, $\omega = 215$ MeV) kinematics. At such perpendicular kinematics FSI effects are predicted to obscure the minimum.

Experiment E97-111 [24] ran two years ago, designed to resolve the issues of the predicted minimum and of reaction mechanism effects. Three kinematics were selected, all covering the p_m range of the minimum: a constant ($q \approx 1$ GeV/c, $\omega \approx 500$ MeV) kinematics at a much larger

Q^2 value than that of the NIKHEF [23] experiment (0.11 $(\mathrm{GeV}/c)^2$) and two parallel kinematics at Q^2 values of 0.8 and 1.9 $(\mathrm{GeV}/c)^2$. The analysis is still in progress, but an on-line analysis showed no indication of a minimum.

In a recently approved experiment, E01-108 [25], a detailed study will be made of the $^4\mathrm{He}(e,e'p)\tau$ reaction at high Q^2 values in kinematics similar to those of the E89-044 experiment. Laget [18] has extended his diagrammatic approach to ^{4}He, so that the results of E01-108 will serve as a benchmark test of his calculations.

5 Polarization transfer

Polarization transfer in the $(\vec{e},e'\vec{p})$ reaction on a proton target provides a direct measure of the ratio of the charge and magnetization form factors of the proton [26]. When studied on a nuclear target, the polarization transfer observables are sensitive to the form factor ratio of a proton embedded in the nuclear medium.

In experiment E89-033 [27] polarization transfer was measured in the reaction $^{16}\mathrm{O}(\vec{e},e'\vec{p})^{15}\mathrm{N}$, the first such measurement in a nucleus other than deuterium. It was the first experiment to use a polarized beam at Jefferson Lab and to use the Focal-Plane Polarimeter (FPP) [28] in Hall A. Electrons from the CEBAF accelerator of energy 2.45 GeV and of longitudinal polarization about 30% were scattered from the same waterfall target as described in sect. 3. Protons with a fixed central momentum of 973 MeV/c were detected in the focal-plane array of the hadron spectrometer in coincidence with electrons. Measurements were made in quasi-perpendicular kinematics, corresponding to central p_m values of 85 and 140 MeV/c. The p_m resolution was sufficient to easily separate the $p_{1/2}$ ground state from the strongly excited $p_{3/2}$-state at 6.32 MeV. In the continuum, a broad peak was observed corresponding mainly to knock-out of protons from the $s_{1/2}$-shell.

The polarization of the knocked-out protons resulted in asymmetric azimuthal distributions after scattering in the (carbon) analyzer of the FPP. These distributions, in combination with the beam helicity information, were analyzed to yield the longitudinal and transverse polarization components of the knocked-out protons. Results [29] for the two bound states and for the unbound $s_{1/2}$-state were compared to a variety of calculations by Kelly and Udias. The statistical error ranges between 15 and 30%, while the systematic error on the individual polarization components is about 6%, mainly due to the uncertainty in the beam polarization. Within the experimental errors all DWIA calculations agree with the data. The relativistic effects on the recoil polarization clearly are small in this p_m range. Also the effects of MEC and IC are predicted by various authors to scatter over the same range as the DWIA calculations do.

Four years later a second polarization transfer experiment was carried out in Hall A, E93-049 [30], this time on ^{4}He. The quality of the polarized beam had increased significantly over that period, with the polarization now up to 70% at a current of up to 70 μA. The new experiment measured the polarization transfer and the induced

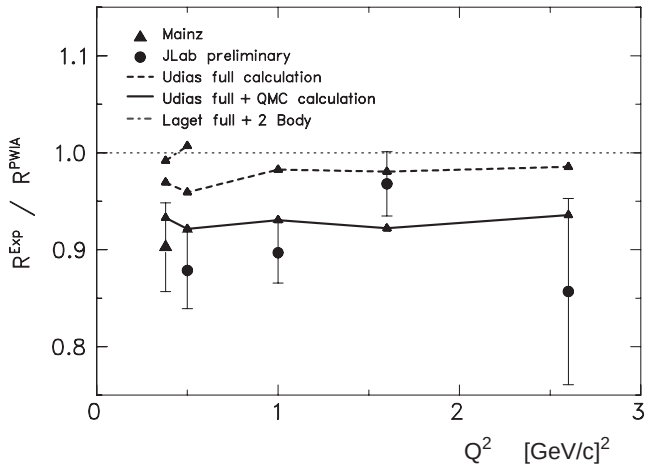

Fig. 6. The super-ratio R/R_PWIA for the reaction $^4\mathrm{He}(\vec{e},e'\vec{p})^3\mathrm{H}$ as a function of Q^2. The dashed curve shows the results of the RDWIA calculation of Udias [5]. The dot-dashed curve represents the result of Laget's full calculation, including two-body currents [18]. The solid curve shows the result of including medium modifications as predicted by a quark-meson coupling model [32] in Udias' RDWIA calculations.

polarization coefficients over the range of Q^2 from 0.5 to 2.6 $(\mathrm{GeV}/c)^2$ and over a range of p_m from 0 to 240 MeV/c. Thanks to the improved quality of the polarized beam, the statistical error now ranged from 4 to 10% with a systematic error of less than 2% in the ratio of the transverse and longitudinal polarization components (P'_x/P'_z) [31]. A ratio R is then defined as

$$R = \frac{(P'_x/P'_z)_{^4\mathrm{He}}}{(P'_x/P'_z)_{^1\mathrm{H}}}\,, \tag{9}$$

and compared to RDWIA calculations by Udias, averaged over the instrumental acceptance (fig. 6).

At $Q^2 = 0.5$ and 1.0 $(\mathrm{GeV}/c)^2$ plane-wave calculations overestimate the data by $\sim 10\%$, while the RDWIA calculations yield $a \sim 3\%$ smaller value for R. Lu *et al.* [32] have predicted a sizeable effect of the nuclear medium on this polarization ratio in a quark-meson coupling model, with the largest effect predicted on the magnetic form fator. Similar effects have been calculated by Frank *et al.* [33] in a light-cone constituent-quark model. Indeed, including the predictions of Lu in the RDWIA calculation results in an excellent agreement with the data. The induced polarization P_y was also extracted from the data. P_y is identically zero in the absence of FSI effects and thus constitutes an excellent test of the validity of the calculated FSI corrections. Indeed, the calculated values of P_y are in good agreement with the data. In summary, the results of experiment E93-049 provide strong evidence for medium modification of the proton form factor ratio.

The author expresses his gratitude to the spokespersons of the experiments presented in this paper for providing him with detailed information. This work was supported by DOE contract

DE-AC05-84ER40150 under which the Southeastern Universities Research Association (SURA) operates the Thomas Jefferson National Accelerator Facility.

References

1. J. Alcorn *et al.*, submitted to Nucl. Instrum. Methods Phys. Res. A.
2. C.W. Leemann, D.R. Douglas, G.A. Krafft, Annu. Rev. Nucl. Part. Sci. **51**, 413 (2001).
3. W. Bertozzi *et al.*, Jefferson Lab experiment E89-003.
4. J. Gao *et al.*, Phys. Rev. Lett. **84**, 3265 (2000).
5. J.M. Udias, J.R. Vignote, Phys. Rev. C **62**, 034302 (2000) and private communication (2002).
6. M.M. Sharma, M.A. Nagarajan, P. Ring, Phys. Lett. B **312**, 377 (1993).
7. E.D. Cooper *et al.*, Phys. Rev. C **47**, 297 (1993).
8. J.J. Kelly, Phys. Rev. C **56**, 2672 (1997).
9. N. Liyanage *et al.*, Phys. Rev. Lett. **86**, 5670 (2001).
10. J.J. Kelly, Phys. Rev. C **60**, 044609 (1999).
11. S. Janssen *et al.*, Nucl. Phys. A **672**, 285 (2000); J. Ryckebusch, private communication (2002).
12. W. Bertozzi *et al.*, Jefferson Lab experiment E00-102.
13. M.K. Jones, P. Ulmer, Jefferson Lab experiment E94-004.
14. P.E. Ulmer *et al.*, Phys. Rev. Lett. **89**, 062301 (2002).
15. F. Ritz *et al.*, Phys. Rev. C **55**, 2241 (1997).
16. W. Boeglin *et al.*, Jefferson Lab experiment E01-020.
17. W. Bertozzi *et al.*, Jefferson Lab experiment E89-044.
18. J.M. Laget, Phys. Rev. D **579**, 333 (1994) and private communication (2002).
19. J.M. Laget, *Proceedings of NATO ASI on New Vistas in Electro-Nuclear Physics* (Plenum Press, New York, 1986) p. 361.
20. A. Kievsky *et al.*, Phys. Rev. C **56**, 64 (1997).
21. S. Tadokoro *et al.*, Prog. Theor. Phys. **78**, 732 (1987).
22. R. Schiavilla, Phys. Rev. Lett. **65**, 835 (1990).
23. J.J. van Leeuwe *et al.*, Phys. Rev. Lett. **80**, 2543 (1998).
24. B. Reitz, J. Templon, J. Mitchell, Jefferson Lab experiment E97-111.
25. K. Aniol *et al.*, Jefferson Lab experiment E01-108.
26. M.K. Jones *et al.*, Phys. Rev. Lett. **84**, 1389 (2000).
27. C.C. Chang *et al.*, Jefferson Lab experiment E89-033.
28. V. Punjabi *et al.*, submitted to Phys. Rev. C.
29. S. Malov *et al.*, Phys. Rev. C **62**, 057302 (2000).
30. R. Ent, P. Ulmer, Jefferson Lab experiment E93-049.
31. S. Strauch *et al.*, submitted to Phys. Rev. Lett., nucl-ex/0211022.
32. D.H. Lu *et al.*, Phys. Rev. C **60**, 068201 (1999).
33. M.R. Frank, B.K. Jennings, G.A. Miller, Phys. Rev. C **54**, 920 (1996).